IEEE Access
Multidisciplinary ⋮ Rapid Review ⋮ Open Access Journal

Received 28 February 2023, accepted 13 March 2023, date of publication 22 March 2023, date of current version 19 July 2023.

Digital Object Identifier 10.1109/ACCESS.2023.3260629

RESEARCH ARTICLE

Analysis of Transformer Winding Deformation and Its Locations With High Probability of Occurrence

HUJUN SHANG[1], XI OUYANG[1], QUAN ZHOU[1,2], JUNFENG DAI[1], AND JIAJIA ZHENG[1]

[1]School of Electrical Engineering, Chongqing University, Chongqing 400044, China

[2]State Key Laboratory of Power Transmission Equipment and System Security and New Technology, Chongqing University, Chongqing 400044, China

Corresponding author: Quan Zhou (zhouquan@cqu.edu.cn)

This work was supported by the National Natural Science Foundation of China under Grant U1866603.

ABSTRACT Power transformer, as a crucial equipment for power transmission, frequently suffers winding deformation defects, owing to the impact of huge external short-circuit current in actual operation. To resist the rapid deterioration of the defects, online monitoring for winding states is imperative, depending on a thorough understanding of the deformation defects. Unfortunately, there are not much related research on the deformation form and location, as two key objects online diagnosed. In this paper, we concentrate on the analysis of winding deformation and investigation of its high-probability location to deeply understand the winding deformation. For the form of the deformation, a three-dimensional finite element model of the transformer is established to obtain the form and extent of the short-circuit impact force, and a buckling model of the low-voltage winding is designed to analyze the mechanism and form of winding deformation under the impact of huge force induced by short-circuit current. For the location of the deformation, the three-dimensional simulation models are established to analyze the force characteristics of different winding structures in three locations (the conductor transposition area, the area with imbalanced amp-turns and the area with uneven circumferential distribution of force). Then we clarify the possibility of winding deformation in these areas, defined as high-probability locations. Finally, the analyzed results are found to be highly consistent with the actual winding deformation, demonstrating the correctness of the research methods and conclusions. Next stage, the results will provide effective theoretical support for online diagnosis of winding deformation and optimal design of winding structure.

INDEX TERMS Winding deformation, electromagnetic force, buckling analysis, high probability site.

I. INTRODUCTION

Power transformers are essential for the transfer of electrical energy, and the dependability of the power supply is directly impacted by the operational status of transformers [1]. Greater demands are placed on the dependable and stable operation of transformers as a result of the growth of power systems and the increasing capacity and voltage levels of transformers [2]. In actual operation, transformers are inevitably prone to a variety of faults or even overall failure. The relevant literature [3] states that winding faults, with winding deformation being the most typical, are among the most frequent faults in transformers. One of the most efficient ways to stop fault deterioration and raise the operational dependability of transformers is to thoroughly analyze the winding deformation mechanism and deterioration process and, as a result, build appropriate monitoring techniques.

Currently, transformer deformation faults are mainly studied by means of numerical analysis, which has the advantage of low cost and high timeliness. The huge current generated in the transformer electromagnetic transient process is the main cause of winding deformation. The short-circuit electromagnetic force is significantly greater than the excitation inrush electromagnetic force, according to research [4], [5], [6], [7] that compared and analyzed the winding electromagnetic force and deformation during no-load closing and

The associate editor coordinating the review of this manuscript and approving it for publication was Amin Mahmoudi.

short-circuiting of power transformers. For the complexity of short-circuit electromagnetic force distribution, literature [8], [9], [10] used two-dimensional and three-dimensional models to analyze the distribution law of short-circuit electromagnetic force on conventional transformer windings, and found that the axial force at the end of the winding was the largest, and the radial force near the middle of the winding was the largest. High-temperature superconducting (HTS) transformers have the advantages of small size, light weight and high efficiency, but they are also more susceptible to short-circuit electromagnetic forces. In the literature [11], [12], [13], [14], the electromagnetic force distribution in HTS transformers is analyzed by means of the finite element method, and the multi-segment winding method and its structural parameter optimization are used to effectively reduce the impact of axial short circuit forces. According to research published in the literature [15], [16], which examined the deformation pattern of windings under short-circuit impact, the radial force is greater in low-voltage (LV) windings, which are more prone to the radial inward concave deformation, and relatively less in high-voltage (HV) windings. The literature [17] analyzed the cumulative strain-stress characteristics of transformer windings based on the theory of elastic-plastic mechanics. The influence of winding preload and the elastic modulus of spacer on the severity of winding deformation was examined in the literature [18], [19]. In the literature [20], the short-circuit resistance of transformer windings and the number of impact withstood were evaluated and analyzed, taking into account initial defects. In conclusion, the existing literature concentrates on the calculation of the magnitude of short-circuit electromagnetic force and the degree of winding deformation, and the current research still has following deficiencies:

1) The mechanism and specific form of winding deformation are less studied. The rapid deterioration of winding defects can be effectively prevented by online monitoring and defect identification [21], which strongly rely on the variation features of internal physical quantities (such as internal magnetic leakage) before and after the winding deformation. However, it is difficult to accurately reflect the winding deformation through the physical quantity variation because current research has not yet performed a sufficient investigation of the winding deformation form and mechanism.

2) There is a lack of adequate research on the high-probability sites where winding deformation occurs. Currently, the acquisition of physical information inside the transformer is mainly by means of optical fiber sensing, which is costly and difficult to achieve full sensing coverage. However, it is worth noting that large power transformers with diverse winding structures often have some potentially weak support areas and force concentration points, which are high-probability locations of winding deformation. The search for high-probability sites of deformation is necessary for the optimal layout of monitoring sensors and the delineation of key monitoring areas.

To perfect the deficiency of existing studies, we conduct the analysis of winding deformation and investigation of its high-probability locations to deeply understand the winding deformation. First, the finite element simulation (FEM) is utilized to analyze the form and degree of winding impact force induced by the short-circuit current. Then, a buckling model of LV winding with the weakness of the local support structure is designed to analyze the mechanism and form of winding deformation under the analyzed impact force. Moreover, 3D simulation models are established to analyze the force characteristics of different winding structures in three locations (the conductor transposition area, the area with imbalanced amp-turns and the area with uneven circumferential distribution of force). Meanwhile, the possibility of winding deformation in these areas are clarified to define the high-probability locations. Finally, to certify the correctness of the methods and conclusions, we compare the analyzed results with the actual winding deformation.

II. WINDING DEFORMATION OF POWER TRANSFORMER

Transformer winding deformation is mainly caused by the short-circuit force impact, thus it is important to fully understand the form and degree of short-circuit impact as well as its distribution law. The analysis of the short-circuit force reveals that the impact force of the short-circuit is greatest in the middle of the LV winding, a compression force inwards along the radius direction, which is more likely to cause winding deformation in actual operation, and the deformation mechanism is more complex [22]. As a result, the focus of this paper is on the radial deformation of LV winding. Considering the complexity of the winding structure and the limited capability of computing equipment, the transformer electromagnetic-mechanical process is decoupled and the electromagnetic force distribution is first accurately calculated using the field-circuit coupling method, and then the mechanical deformation process is calculated in the structural field, which further reduces the complexity of the calculation while ensuring that the calculation is in line with reality.

A. DISTRIBUTION OF SHORT-CIRCUIT ELECTROMAGNETIC FORCE

A 35 kV three-phase transformer is modeled in a three-dimensional simulation. The basic parameters of the transformer are shown in Table 1, and the material properties of the transformer components are shown in Table 2. The field - circuit coupling method is used to simulate the external three-phase symmetrical short circuit fault of the transformer, and then the short circuit electromagnetic force on the winding is calculated. Considering the symmetry of the three-phase winding, only the B-phase winding is taken here for the analysis of the short-circuit electromagnetic force.

The spatiotemporal distribution of the short-circuit electromagnetic force along the winding height is shown in Figure 1. It can be seen that the maximum electromagnetic force on the winding is reached at 0.01 seconds after the occurrence

TABLE 1. Parameters of the power transformer.

Classification	Value
capacity	2500 kVA
rated voltage	38.5 / 10.5 kV
short circuit impedance	7.47 %
winding turns of HV/LV	525/272
inner diameter of HV winding	410 mm
out diameter of HV winding	505 mm
inner diameter of LV winding	285 mm
out diameter of LV winding	330 mm

TABLE 2. Parameters of Transformer material.

Components	Winding	Core
material	copper	silicon steel
elastic modulus	119 GPa	190 GPa
poisson ratio	0.34	0.3
density	8900 kg/m^3	7800 kg/m^3
conductivity	5×10^7 S/m	2×10^6 S/m
relative permeability	1	5000

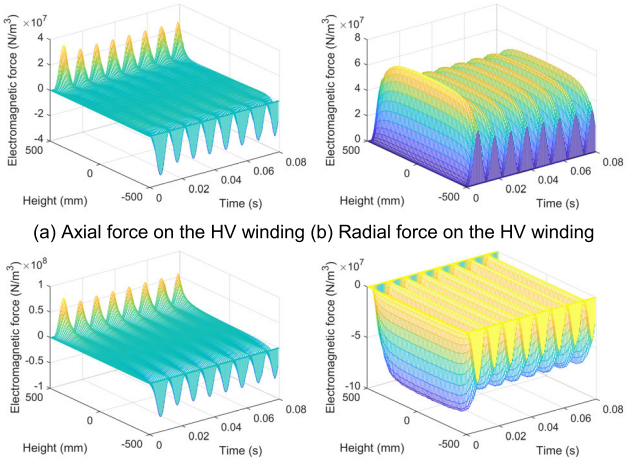

(a) Axial force on the HV winding (b) Radial force on the HV winding

(c) Axial force on the LV winding (d) Radial force on the LV winding

FIGURE 1. Distribution of short-circuit electromagnetic force.

of short circuit. The maximum radial forces of the HV and LV windings can reach 4.2×10^7 N/m^3 and 1.05×10^8 N/m^3 respectively, and the maximum axial forces reach 2.5×10^7 N/m^3 and 8.2×10^7 N/m^3 respectively. The radial force is symmetrically distributed in space, peaking at the middle height of winding and decreasing with winding height as it approaches the top and lower ends. The radial electromagnetic force in the HV winding is a tensile force that tends to increase the radius of the winding along the radius direction outwards; the radial force in the LV winding is a compressive force that tends to decrease the radius of the winding along the radius direction inwards. The axial force applied to the winding ends is the greatest and the upper and lower ends are subjected to different directions of force. The winding is compressed from the two ends towards the middle as a result of an axial electromagnetic force acting downwardly on the top end and upwardly on the lower end of the winding.

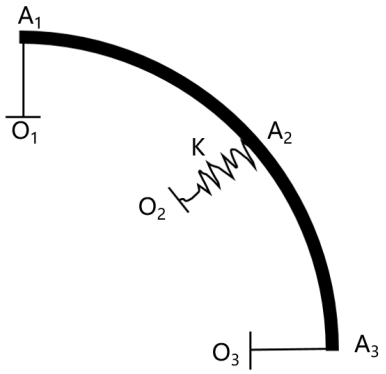

FIGURE 2. Radial buckling model combining elastic and fixed braces for LV winding.

The greatest short-circuit impact force, based on the study above, appears at the middle height of the winding and operates on the winding conductor in a radial direction. The HV winding experiences radial tensile stress when the radial impact force is applied to it; the LV winding, however, experiences radial compressive stress, which is significantly greater than that of the HV winding and is more likely to result in winding deformation.

B. DEFORMATION ANALYSIS OF LV WINDING

Radial deformation of LV winding is a buckling deformation under pressure. Considering that the winding braces may not be fixed completely, a radial buckling model combining elastic and fixed braces for LV winding is established in this paper to calculate the critical loads and buckling deformation form (vibration patterns) of the windings. Furthermore, to identify the deformation process of the winding, its post-buckling stage is tracked by measuring the reaction force with the specified winding displacement.

The radial buckling model with both fixed and elastic braces is depicted in Figure 2. A quarter of the winding is modelled with fixed supports at both ends and elastic supports in the middle to simulate the weakened strength of the local braces. The constraint for fixed node Oi is that both translational and rotational displacements are zero, and the constraint for support node Ai is that all displacements other than radial displacements are zero.

The critical load and deformation pattern of winding structure can be provided by the buckling analysis. The winding structure has an incremental balance equation at steady state as shown in equation (1).

$$([K]_0 + \lambda [K]_\delta)[\Delta q] = [\Delta S] \tag{1}$$

where $[K]_0$ is the initial stiffness matrix, $[K]_\delta$ is the initial stress matrix, Δq is the displacement increment, ΔS is the load variation. When the winding structure is in the critical instability state, if a small load disturbance is applied, the structure will rapidly undergo a large deformation, and the corresponding load is called buckling load or critical load [23]. This indicates that the load variation of incremental

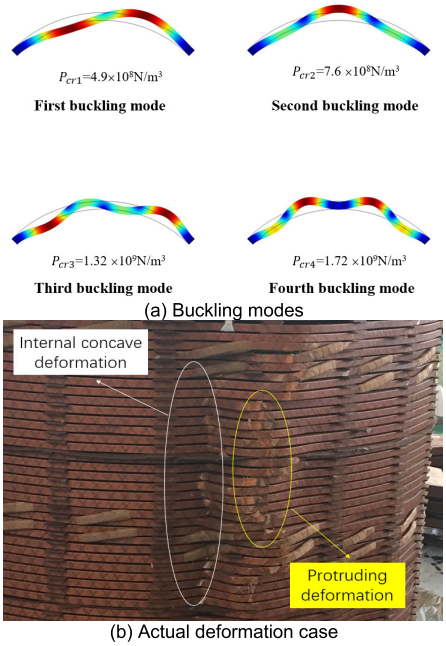

FIGURE 3. The form of winding deformation.

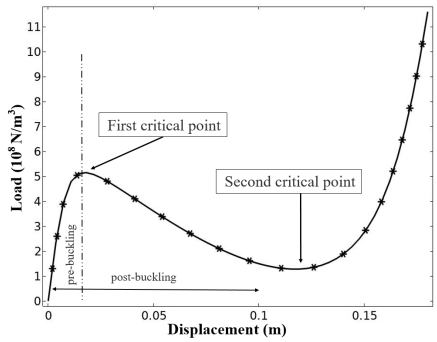

FIGURE 4. The load - displacement curve.

balance equation is approximately equal to zero. Therefore, the eigenvalue λ can be obtained according to the following formula:

$$\det([K]_0 + \lambda [K]_\delta) = 0 \tag{2}$$

The critical buckling load P_{cr} is obtained by multiplying the eigenvalue λ by the initial load P_0. The critical loads for each order mode of the winding structure are obtained from the buckling analysis as 4.9×10^8 N/m^3, 7.6×10^8 N/m^3, 1.32×10^9 N/m^3 and 1.72×10^9 N/m^3. Figure 3a depicts the buckling modes of winding when the middle brace is not completely fixed. Figure 3b shows the actual deformation case of the LV winding, which is related to the winding structure and the support strength of the brace. The winding deformation form is typically the first-order mode in Figure 3a, with some protruding deformation near the concave deformation in the winding, which is basically consistent with the actual deformation case shown in Figure 3b.

The critical buckling load can be predicted by linear buckling analysis, but it is unable to provide the deformation condition above the critical load. Post buckling analysis is the process of tracing the solution in the situation of above critical load. In this paper, the post-buckling process of the winding structure is tracked by specifying the winding displacement and then measuring the reaction force, and the load-displacement curve obtained is shown in Figure 4.

Two critical points can be observed in Figure 4, the first of which occurs near a load equal to 5.0×10^8 N/m^3, which is essentially the same as the first-order critical load value of 4.9×10^8 N/m^3 obtained from the buckling analysis. At this point, the deformation of the winding reaches 0.016m, the winding structure becomes unstable and post-buckling occurs. As the deformation increases the required load value decreases, and when the deformation of the winding structure increases to 0.12m the load has already decreased to 1.3×10^8 N/m^3. At this point, a second critical point is reached and the winding structure enters a new stable configuration, after which the larger load is required for the larger deformation displacement.

III. HIGH-PROBABILITY SITES OF DEFORMATION

The winding structure of large power transformers is complex and diverse, and there are often some areas with mechanical weakness and stress concentration, which are more prone to winding deformation. Therefore, such positions can be regarded as the sites with high probability of winding deformation. The online monitoring of winding deformation defects not only depends on the understanding of winding deformation form but also needs to fully grasp the high-probability site of deformation defects so as to optimize the layout of monitoring sensors and divide key monitoring areas.

In this paper, the 3D simulation models are established to analyze the force characteristics of different winding structures in three locations (the conductor transposition area, the area with imbalanced amp-turns and the area with uneven circumferential distribution of force), so as to obtain the mechanical weak points of the windings and to explore the sites with a high probability of winding deformation.

A. CONDUCTOR TRANSPOSITION AREA

Transposition between the conductors is commonly necessary to limit the ring current in LV windings, which are often spiral winding with multiple conductors in parallel. The distribution of the winding electromagnetic force is impacted by the transposition, which alters the spatial layout of the conductors and distorts the distribution of leakage flux. Moreover, in the area of conductor transposition, there is usually an asymmetry in the spatial structure of the winding, which makes it prone to local deformation.

A three-phase transformer is used as a research object to analyze the law of electromagnetic force distortion in the area of LV winding transposition. The rated parameters of the transformer and its constructional characteristics are shown in Table 3. In order to save calculation memory, only the MV

TABLE 3. Parameters of the 110kV transformer.

Classification	Value
capacity	12500 kVA
rated voltage	110 / 38.5 / 10.5 kV
short circuit impedance	6.29 %(M-L)
winding turns of HV/MV/LV	398/139/38
inner/ out diameter of LV winding	620 / 740 mm
position of conductor transposition	at 1/2 height of winding
number of conductor in LV winding	2

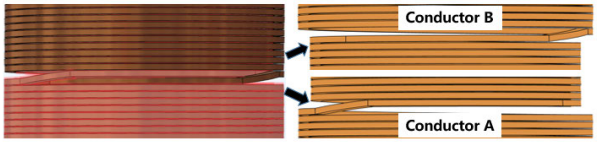

FIGURE 5. The refined model of LV winding and its transposition structure.

and LV windings of phase B are modelled in this section, ignoring the HV and regulating windings. The structure of finely modeled LV winding and conductor transposition area is shown in Figure 5. The process of winding transposition can be summarized as follows: before transposition, conductor A and B are located on the outside (near the MV winding) and inside (near the core) of the LV winding; after transposition, the positions of the two conductors are swapped. In the first stage of the transposition of conductor A, the radius of wire rotation remains unchanged and the height increases rapidly, but in the second stage, the height of the conductor increases at the same rate as before the transposition, and the radius decreases gradually. The transposition process of conductor B is the opposite of conductor A, first reducing the radius and rotating inwards, and then raising the height.

The distribution of electromagnetic force on the LV winding is depicted as a cloud diagram in Figure 6. As can be observed, the distribution of radial force at the transposition structure is almost unaltered, while the axial force distribution is seriously distorted near the transposition area, even changing the force direction of the winding. And the distortion is not only present in the transposition structure itself, but also has an effect on the upper and lower three turns of the conductor in its vicinity. This is due to a surge in local radial leakage brought on by the gap of transposition structure, which leads an increase of axial electromagnetic force. The distribution of the axial leakage is essentially unaffected by the transposition structure so that the radial electromagnetic force remains almost unchanged.

Figure 7 shows the change in electromagnetic force before, during and after the transposition of the two conductors. The axial and radial components of the electromagnetic force are almost constant before and after the transposition. Before the transposition, the radial electromagnetic forces of conductor A and B are $7.2 \times 10^5 \mathrm{N/m^3}$ and $2.6 \times 10^5 \mathrm{N/m^3}$ respectively; after the transposition, the radial electromagnetic forces of conductor A and B are $2.6 \times 10^5 \mathrm{N/m^3}$ and $7.3 \times 10^5 \mathrm{N/m^3}$.

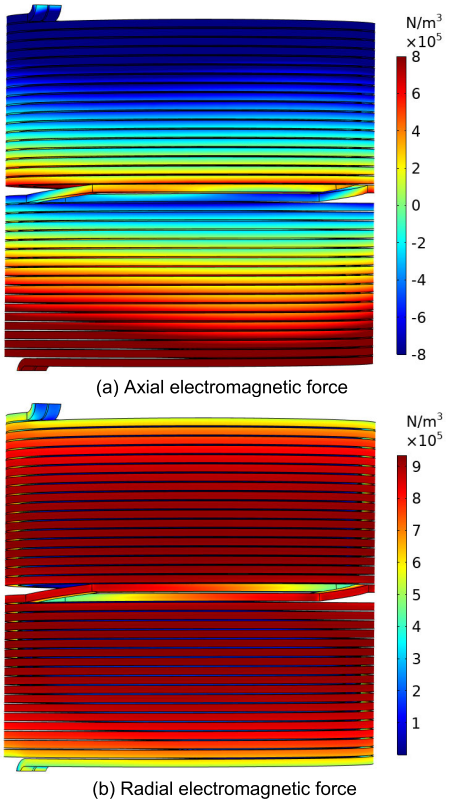

FIGURE 6. Cloud diagram of the electromagnetic force distribution in the LV winding.

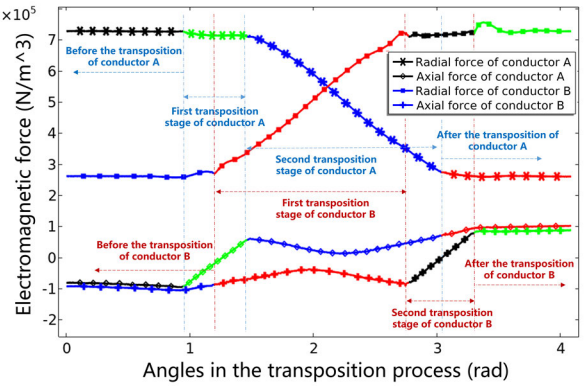

FIGURE 7. Curve of the electromagnetic force during transposition.

In the first transposition stage of conductor A, the radial electromagnetic force decreases slowly, and in the second transposition stage, the radial force decreases sharply to 1/3 of that before transposition. During the first and second transposition of conductor B, the radial electromagnetic force changes in the opposite direction to that of conductor A, first increasing sharply and then slowly rising to about three times the level before the transposition. The axial electromagnetic forces of conductor A and B are respectively $-0.9 \times 10^5 \mathrm{N/m^3}$ and $-1 \times 10^5 \mathrm{N/m^3}$ before the transposition, and they are respectively $1 \times 10^5 \mathrm{N/m^3}$ and $0.9 \times 10^5 \mathrm{N/m^3}$ after the transposition. In the first stage of the transposition process, the

TABLE 4. Different cases for the distribution of the tap winding.

Classification	Location of the tap winding
Case A	No tap winding
Case B	Top and bottom ends of the winding
Case C	Top end of the winding
Case D	Middle height of the winding
Case E	1/4 and 3/4 height of the winding

axial electromagnetic force of conductor A decreases first and then increases in the reverse direction; in the second stage, the electromagnetic force decreases and then increases. The axial force variation trend of conductor B is symmetrical and opposite to that of conductor A during the transposition process.

At the transition point between the first and second stages of the transposition process, the axial force acting on the conductor is at its greatest. This spot can be thought of as a high-probability position for axial deformation of the winding due to the quick change in height of the conductor at this location and the fact that the conductor is subjected to strong axial force in opposite directions over a very short length. In the non-transposition area, the two conductors are wound side by side in parallel and they can be considered as a single unit in terms of strength. Due to the balance of stresses within the conductors, the actual radial electromagnetic force applied to each conductor is approximately the average of the electromagnetic forces of the two conductors (4.9×10^5 N/m^3). In the first transposition stage of conductor A and the second stage of conductor B, the magnitude of radial electromagnetic force on the conductor is slightly reduced compared to the pre-transposition stage (approximately 7.15×10^5 N/m^3), but at this point conductor A and B are no longer twisted side by side and only one conductor exists in the same radial space, with the conductor being subjected to a greater radial force at this stage. Therefore, the first and second stages of the conductor transposition are the high-probability locations for the radial deformation of the winding.

B. THE AREA WITH UNBALANCED AMP-TURNS

The transformer is assumed to have a uniform distribution of amp-turns along the winding height direction in the existing analysis of electromagnetic force. In practice, due to the presence of the tap winding in HV winding, the distribution of amp-turns along the axial direction of the HV and LV windings is actually unbalanced. These unbalanced amp-turns will distort the distribution of the radial leakage and thus change the electromagnetic force in the winding [24], [25].

In this paper, the distribution of electromagnetic force for the five scenarios in Table 4 is analyzed on the basis of the 3-D simulation model of the transformer built in section II-A. The location of the tap winding is shown in Figure 8, where the amp-turns unbalance factor a is expressed as a percentage of the number of unbalanced amp-turns to the total number of amp-turns, all of which are 10 % in this study.

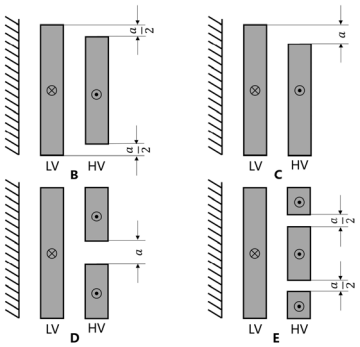

FIGURE 8. Distribution of tap winding positions.

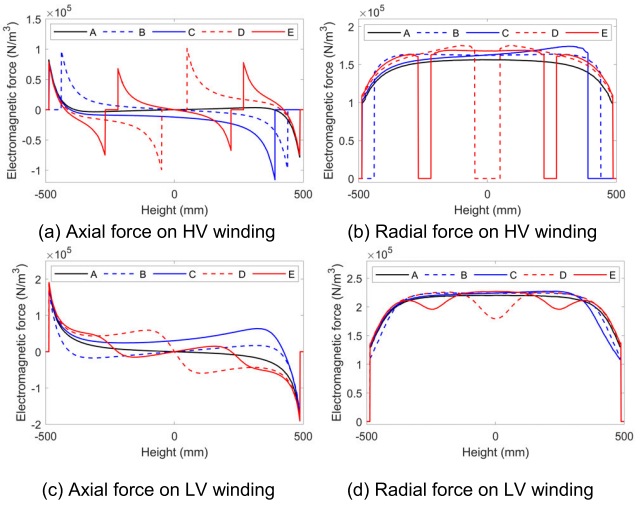

FIGURE 9. Distortion of the electromagnetic force distribution in the region with unbalanced amp-turns.

Figure 9 shows the distortion of the electromagnetic force distribution on the HV and LV windings when the tap winding is located in different parts of the HV winding. The unbalance of ampere-turns has the greatest influence on the axial force of HV winding, which is mainly reflected in the change of the maximum value and symmetry of axial force. When the tap winding is at top end of the HV winding, the axial force distortion is the most serious, the maximum value becomes 1.53 times of that without tap winding, and the symmetry of the force distribution is seriously damaged. When the tap winding is located at top end of the winding, it also has the greatest influence on the axial force of the LV winding and the radial force of the HV winding. The amplitude variation of the axial force on the LV winding is up to 40926 N/m^3, and the direction of the force also changes. The distortion degree of radial force on the HV winding can reach 19.7 %. When the tap winding is located in the middle of the winding, it has the greatest influence on the radial force of the LV winding, and the degree of distortion can reach 18.6 %.

The axial force of winding in the area with unbalanced amp-turns is greatly increased, so this area is a high-probability location for axial bending deformation of the winding. It is worth noting that when the tap winding is

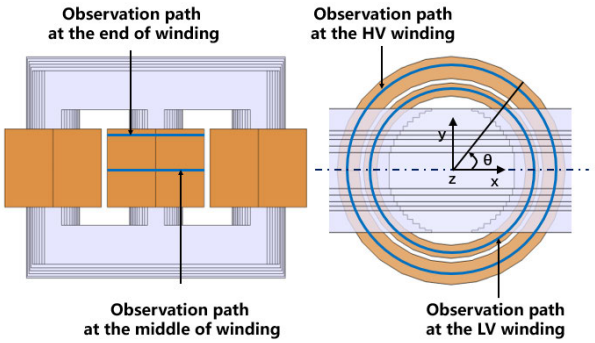

FIGURE 10. The transformer model and observation path.

located at one end of the high voltage winding, the unbalanced amp-turns destroy the symmetry of the axial force distribution and make axial displacement of the winding and axial compression deformation at the end more likely to occur.

C. THE AREA WITH UNEVEN CIRCUMFERENTIAL DISTRIBUTION OF FORCE

Influenced by the adjacent phase currents, there are differences in electromagnetic forces at different locations on the circumference of the winding. At the same time, the leakage magnetic field at the end of the winding is greatly affected by the yoke, which leads to the difference of the electromagnetic force on the winding inside and outside the core window, and determines the probability of winding deformation at different positions to some extent.

A 3-D simulation model of the 110 kV transformer has been built based on the actual parameters shown in Table 3 of Section III-A, as shown in Figure 10. As phase effects have to be taken into account, the way in which only the B-phase winding was modelled in section III-A can no longer be used. Therefore, in order to reduce the amount of calculations, the LV winding is also no longer modelled in a refined way, but in a cylindrical configuration instead.

Figure 11 shows the distribution of electromagnetic forces along the circumference of winding. The circumferential unevenness of the electromagnetic force distribution is mainly caused by difference in the magnetic field distribution inside and outside the core window and by the effect of magnetic leakage flux from adjacent phase windings.

For the B-phase winding, the uneven distribution of electromagnetic forces is mainly due to the difference of the magnetic field distribution inside and outside the window, and this difference mainly affects the distribution of electromagnetic forces at the end of the winding. As can be seen from Figures 11-a and 11-b, the radial and axial electromagnetic forces in the window at the end of the HV winding are 7.9×10^4 N/m^3 and 1.7×10^4 N/m^3, respectively, which are 23 % and 42 % higher than those outside the window (6.4×10^4 N/m^3, 1.2×10^4 N/m^3). Figures 11-c and 11-d

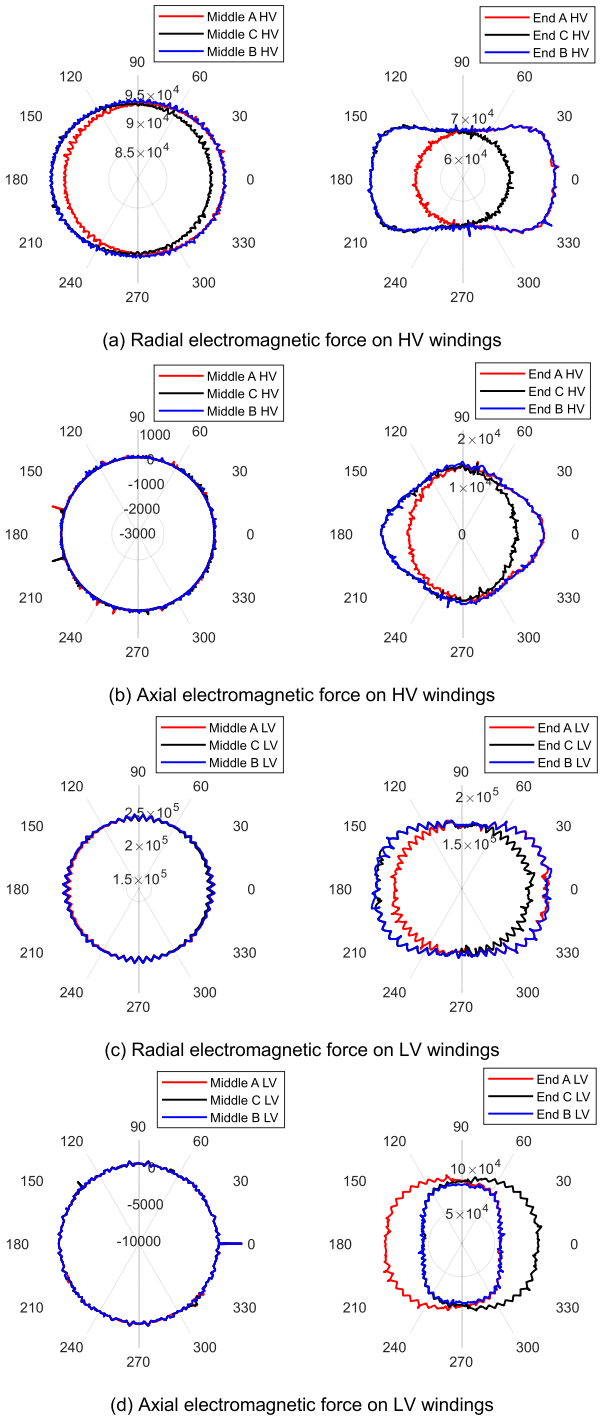

FIGURE 11. Circumferential distribution of electromagnetic force.

show that the radial force inside the window at the end of the LV winding is 2.0×10^5N/m^3, 25 % higher than that outside the window (1.6×10^5 N/m^3), while the axial force inside the window is 5.2×10^4N/m^3, 36 % lower than that outside the window (8.2×10^4N/m^3).

For the A- phase and C-phase windings, the circumferential distribution of electromagnetic force is not only affected by the difference between the magnetic field inside

and outside the window, but also affected by the magnetic leakage of the adjacent windings (B-phase). Among them, the difference of the electromagnetic force in the middle of phase A and C windings is relatively small. As shown in Figure 11-a, in the middle of the HV winding, the radial force of phase A and C winding near the B phase winding is $9.6 \times 10^4 \mathrm{N/m^3}$, 4 % higher than that of the radial force (9.2×10^4 N/m^3) far away from the B phase winding. The difference of the electromagnetic force at the end of phase A and C windings is relatively large. Figures 11-a and 11-b show that, the circumferential distribution deviations of the radial and axial electromagnetic forces at the end of the HV windings are 25 % and 68 %, respectively; Figures 11-c and 11-d show that the distribution deviations of the radial and axial forces at the end of the LV windings are 28 % and 104 %, respectively.

According to the above analysis, it can be concluded that: the area of B-phase HV winding inside the window is the high-probability site of radial convex deformation and axial bending deformation; the area inside and outside the window of LV winding is the high-probability site of radial buckling deformation and axial bending deformation respectively; for A-phase and C-phase windings, although the electromagnetic force is smaller than that of B-phase winding, the difference of its circumferential distribution is much larger than that of B-phase winding, so they are more prone to side shift and axial tilt collapse.

IV. CONCLUSION

This paper focuses on the analysis of transformer winding deformation and research on the locations with high probability of deformation, with the following works done.

1)The short-circuit electromagnetic forces on the windings have been analyzed using the field-circuit coupling method. Specifically, the force reaches the maximal value at half a cycle after the short circuit occurs. At the moment, maximum stress locates at the middle height of the LV winding, and presents as a compression force inwards along the radius direction.

2)The buckling deformation model of LV winding with the small-deflection is developed to calculate the critical loads and buckling deformation form (vibration patterns) of the windings. Conclusively, the obtained form is observed to closely match the actual cases. Furthermore, to identify the deformation process of the winding, its post-buckling stage is tracked by measuring the reaction force with the specified displacement.

3)The force characteristics of windings at three areas are analyzed by 3-D FEM simulation to determine the location where the defects are easily induced. As the results, the conductor transposition structure is found as a high-probability location for the radial deformation of the winding. The areas with unbalanced amp-turns are prone to axial bending deformation and axial compression deformation. Besides, the area inside the core window is highly potential to occur the winding deformation.

Next stage, all research results can provide effective theoretical support for online identification of winding deformation defects and optimal design of winding structures.

REFERENCES

[1] C. Chen, X. Jianyuan, L. Xin, and L. Xiaolong, "State diagnosis method of transformer winding deformation based on fusing vibration and reactance parameters," *IET Electric Power Appl.*, vol. 14, no. 5, pp. 818–826, May 2020, doi: 10.1049/iet-epa.2019.0564.

[2] M. Bagheri, A. Zollanvari, and S. Nezhivenko, "Transformer fault condition prognosis using vibration signals over cloud environment," *IEEE Access*, vol. 6, pp. 9862–9874, 2018, doi: 10.1109/access.2018.2809436.

[3] C. Aj, M. A. Salam, Q. M. Rahman, F. Wen, S. P. Ang, and W. Voon, "Causes of transformer failures and diagnostic methods—A review," *Renew. Sustain. Energy Rev.*, vol. 82, pp. 1442–1456, Feb. 2018, doi: 10.1016/j.rser.2017.05.165.

[4] J. Faiz, B. M. Ebrahimi, and T. Noori, "Three- and two-dimensional finite-element computation of inrush current and short-circuit electromagnetic forces on windings of a three-phase core-type power transformer," *IEEE Trans. Magn.*, vol. 44, no. 5, pp. 590–597, May 2008, doi: 10.1109/tmag.2008.917819.

[5] C. Zhang, W. Ge, Y. Xie, and Y. Li, "Comprehensive analysis of winding electromagnetic force and deformation during no-load closing and short-circuiting of power transformers," *IEEE Access*, vol. 9, pp. 73335–73345, 2021, doi: 10.1109/access.2021.3068054.

[6] W. D. S. Fonseca, D. de S. Lima, A. K. F. Lima, N. S. Soeiro, and M. V. A. Nunes, "Analysis of electromagnetic-mechanical stresses on the winding of a transformer under inrush currents conditions," *Int. J. Appl. Electromagn. Mech.*, vol. 50, no. 4, pp. 511–524, Mar. 2016, doi: 10.3233/jae-150044.

[7] Y. Zhao, T. Wen, Y. Li, H. Ni, Q. Zhang, and W. Chen, "A FEM-based simulation of electromagnetic forces on transformer windings under short-circuit," in *Proc. IEEE Int. Power Modulator High Voltage Conf. (IPMHVC)*, Jackson, WY, USA, Jun. 2018, pp. 425–429.

[8] Z. Li, Z. Hao, C. Yan, Y. Dang, H. Xu, and B. Zhang, "Deformation simulation and analysis of power transformer windings," in *Proc. IEEE PES Asia–Pacific Power Energy Eng. Conf. (APPEEC)*, Xian, China, Oct. 2016, pp. 1445–1449.

[9] H.-M. Ahn, J.-Y. Lee, J.-K. Kim, Y.-H. Oh, S.-Y. Jung, and S.-C. Hahn, "Finite-element analysis of short-circuit electromagnetic force in power transformer," *IEEE Trans. Ind. Appl.*, vol. 47, no. 3, pp. 1267–1272, May 2011, doi: 10.1109/TIA.2011.2126031.

[10] A. Najafi and I. Iskender, "A new approach to reduce the leakage flux and electromagnetic force on distribution transformer under unbalanced faults based on finite element method," *Int. Trans. Electr. Energy Syst.*, vol. 26, no. 4, pp. 901–916, Apr. 2016, doi: 10.1002/etep.2119.

[11] A. Ahmadpour and A. Dejamkhooy, "Modeling and analysis of HTS distribution transformers under various conditions using FEM," *J. Supercond. Novel Magnetism*, vol. 35, no. 7, pp. 1847–1856, Jul. 2022, doi: 10.1007/s10948-022-06210-y.

[12] A. Moradnouri, M. Vakilian, A. Hekmati, and M. Fardmanesh, "Multi-segment winding application for axial short circuit force reduction under tap changer operation in HTS transformers," *J. Supercond. Novel Magnetism*, vol. 32, no. 10, pp. 3171–3182, Oct. 2019, doi: 10.1007/s10948-019-5109-1.

[13] A. Moradnouri, M. Vakilian, A. Hekmati, and M. Fardmanesh, "Optimal design of flux diverter using genetic algorithm for axial short circuit force reduction in HTS transformers," *IEEE Trans. Appl. Supercond.*, vol. 30, no. 1, pp. 1–8, Jan. 2020, doi: 10.1109/tasc.2019.2923550.

[14] A. Moradnouri, M. Vakilian, A. Hekmati, and M. Fardmanesh, "HTS transformers leakage flux and short circuit force mitigation through optimal design of auxiliary windings," *Cryogenics*, vol. 110, Sep. 2020, Art. no. 103148, doi: 10.1016/j.cryogenics.2020.103148.

[15] H. K. Li, "Simulation of power transformer windings displacement caused by multiple short-circuit forces," in *Proc. 2nd Int. Conf. Appl. Mech., Mater. Manuf. (ICAMMM)*, Changsha, China, Nov. 2013, pp. 1341–1344, doi: 10.4028/www.scientific.net/AMM.268-270.1341.

[16] S. Pradhan and S. K. Nayak, "Winding dislocation of a power transformer and its analysis to locate and estimate the deformation," in *Proc. 2nd Int. Conf. Power, Energy Environ., Towards Smart Technol. (ICEPE)*, Shillong, India, Jun. 2018, pp. 1–9.

[17] S. Wang, H. Zhang, S. Wang, H. Li, and D. Yuan, "Cumulative deformation analysis for transformer winding under short-circuit fault using magnetic–structural coupling model," *IEEE Trans. Appl. Supercond.*, vol. 26, no. 7, Oct. 2016, Art. no. 0606605, doi: 10.1109/TASC.2016.2584984.
[18] Y. Chenguang, H. Zhiguo, Z. Song, Z. Baohui, Z. Tao, and L. Zhengyuan, "Computation and analysis of power transformer winding damage due to short circuit fault based on 3-D finite element method," *Int. J. Appl. Electromagn. Mech.*, vol. 51, no. 4, pp. 405–418, Aug. 2016, doi: 10.3233/jae-150163.
[19] S. Wang, S. Wang, H. Li, and D. Yuan, "Dynamic deformation analysis of power transformer windings considering the influence of temperature on elasticity characteristics of winding materials under short circuit fault," *Int. J. Appl. Electromagn. Mech.*, vol. 59, no. 2, pp. 657–668, Mar. 2019, doi: 10.3233/jae-171050.
[20] Z. Bo and L. Yan, "Research on radial stability of large transformers windings under multiple short-circuit conditions," *IEEE Trans. Appl. Supercond.*, vol. 26, no. 7, pp. 1–4, Oct. 2016, doi: 10.1109/tasc.2016.2594843.
[21] Y. Zhoufei, Y. Yi, W. Zhihao, L. Zhe, and W. Qiaohua, "Apparatus for on-line monitoring of transformer winding deformation using leakage inductance identification," in *Proc. IEEE Int. Conf. Condition Monitor. Diagnosis*, Bali, Indonesia, Sep. 2012, pp. 613–616.
[22] Z. W. Zhang, W. H. Tang, T. Y. Ji, and Q. H. Wu, "Finite-element modeling for analysis of radial deformations within transformer windings," *IEEE Trans. Power Del.*, vol. 29, no. 5, pp. 2297–2305, Oct. 2014, doi: 10.1109/TPWRD.2014.2322197.
[23] D. Geibler and T. Leibfried, "Short-circuit strength of power transformer windings-verification of tests by a finite element analysis-based model," *IEEE Trans. Power Del.*, vol. 32, no. 4, pp. 1705–1712, Aug. 2017, doi: 10.1109/TPWRD.2016.2572399.
[24] L. Li, X. Liu, G. Zhu, H. Chen, and S. Gao, "Research of short-circuit performance of a split-winding transformer with stabilizing windings," *IEEE Trans. Appl. Supercond.*, vol. 29, no. 2, pp. 1–6, Mar. 2019, doi: 10.1109/TASC.2018.2889271.
[25] K. Dawood, F. Isik, and G. Kömürgöz, "Analysis and optimization of leakage impedance in a transformer with additional winding: A numerical and experimental study," *Alexandria Eng. J.*, vol. 61, no. 12, pp. 11291–11300, Dec. 2022, doi: 10.1016/j.aej.2022.05.014.

HUJUN SHANG was born in Gansu, China, in 1998. He received the B.S. degree in electrical engineering from Jilin University, China, in 2020. He is currently pursuing the M.S. degree in electrical engineering with Chongqing University, China.

His research interest includes the simulation and numerical analysis of power transformer.

XI OUYANG was born in Jiangxi, China, in 1995. He received the B.S. degree in electrical engineering from the Changsha University of Science and Technology, China, in 2017. He is currently pursuing the Ph.D. degree in electrical engineering with Chongqing University, China.

His research interest includes the theory and technology of insulation condition monitoring and fault diagnosis of electrical equipment.

QUAN ZHOU was born in Chongqing, China, in 1973. He received the B.S., M.S., and Ph.D. degrees in electrical engineering from Chongqing University, Chongqing, in 1994, 1998, and 2004, respectively.

He is currently a Professor with the Department of Electrical Engineering, Chongqing University. His current research interests include the theory and technology of insulation condition monitoring and fault diagnosis of electrical equipment, safety assessment of new energy power equipment, intelligent distribution network optimization, and fault diagnosis.

JUNFENG DAI was born in Hubei, China, in 1997. He received the B.S. degree in electrical engineering from the Wuhan University of Technology, China, in 2020. He is currently pursuing the M.S. degree in electrical engineering with Chongqing University, China.

His research interest includes optical fiber power transmission and communication.

JIAJIA ZHENG was born in Chongqing, China, in 1997. She received the B.S. degree in electrical engineering from Southwestern University, China, in 2019. She is currently pursuing the M.S. degree in electrical engineering with Chongqing University, China.

Her research interests include partial discharge detection and simulation studies of space-charge.